Journal of Computational Physics **172,** 451–471 (2001)
doi:10.1006/jcph.2001.6814, available online at http://www.idealibrary.com on IDEAL®

A Hybrid Finite Element and Integral Equation Domain Decomposition Method for the Solution of the 3-D Scattering Problem

Bruno Stupfel

CEA/CESTA, Commissariat à l'Énergie Atomique, B.P. 2, 33114 Le Barp, France
E-mail: stupfel@bordeaux.cea.fr

Received October 13, 2000; revised April 25, 2001

A domain decomposition method (DDM) is presented for the solution of the time-harmonic electromagnetic scattering problem by inhomogeneous 3-D objects. The computational domain is partitioned into concentric subdomains on the interfaces of which Robin-type transmission conditions are prescribed. On the outer boundary terminating the computational domain, the radiation condition is accounted for by employing an integral equation (IE) formulation. The DDM decouples the interior problems, that correspond to the solution of Maxwell's equations inside each subdomain and are formulated by using a finite element method, from the exterior problem solved by employing the IE. It has been shown that the solutions of this DDM algorithm converge to those of the original problem. A particular IE is used that allows the implementation of a very simple and fully iterative solver. The main advantage offered by this technique is a reduction in memory requirements. Various numerical examples are presented that illustrate its potential. © 2001 Academic Press

Key Words: electromagnetism; Maxwell; absorbing boundary conditions; domain decomposition method; integral equation; finite elements; numerical methods.

I. INTRODUCTION

The scattering problem of a time-harmonic electromagnetic wave from penetrable complex 3-D objects can be accurately solved by employing a hybrid finite element (FE) and integral equation (IE) method [1–5]. A surface S encloses the inhomogeneous, possibly anisotropic, medium constituting the object. S is the outer boundary of the computational domain inside which the fields are formulated using the finite element method. Prescribed on S, the IE constitutes an exact radiation condition that accounts for the propagation in the unbounded and homogeneous surrounding space. Both IE and FE formulations are coupled by enforcing the continuity of the tangential components of the fields on S. The discretization process leads to a linear system constituted, essentially, by a sparse FE matrix and a dense

0021-9991/01 $35.00
Copyright © 2001 by Academic Press
All rights of reproduction in any form reserved.

IE matrix. However, the solution of this system becomes computationally intensive and requires large computer resources when the size of the object is electrically large.

A domain decomposition method (DDM) allows the decomposition of a large problem into several coupled subproblems that can be solved independently, thus reducing the memory storage requirements. It has drawn the attention of a number of researchers in the electromagnetic community, who have devised several methods to deal with the scattering problem. In particular, two classes of methodologies may be identified. In the first one [6–9], no iterations are required but the solutions may not be unique on account of the fact that some subproblems may involve Dirichlet or Neumann boundary conditions. Methodologies of the second class [10–14] are based on an iterative DDM originally proposed in [10, 11]: The fields in two adjacent subdomains are connected by a mixed boundary condition, termed transmission condition (TC), that ensures the uniqueness of the solutions and their convergence to those of the original problem. To improve the efficiency of the TC and, consequently, to reduce the number of iterations, this method has been later adapted to a particular, "onion-like," partition of the computational domain into concentric subdomains circumscribing the object [13, 14], and the convergence of the corresponding modified algorithm has been established in [15]. On account of its local character, an absorbing boundary condition (ABC) that approximates the exact radiation condition has been used on S to further reduce the computing time and memory storage. However, scattering by a stealth object, the bistatic radar cross section (RCS) of which exhibits a large angular dynamic range, can be accurately calculated in the high frequency domain only if the boundary S is placed sufficiently far away from the object, requiring for that reason a large number of subdomains [14, 16]. Hence, it turns out to be necessary to have at one's disposal an "exact" method where the IE is substituted to the ABC.

In this paper, we investigate the numerical capabilities of the hybrid FE–IE DDM proposed in [15]: The unbounded surrounding space in the region exterior to S is considered as an additional subdomain connected to the interior FE region by a TC, while keeping for the latter the subdomains' partition. It offers, a priori, the following advantages:

—The solutions of the FE and IE systems are performed separately: it only remains to choose an IE that can be solved iteratively in an efficient manner.

—The FE system is solved by using the DDM as in [14]. Each partial FE system corresponding to one subdomain is solved with a standard conjuguate gradient (CG).

The organization of this paper is as follows. In Section II we outline the 3-D electromagnetic scattering problem to be solved and the DDM algorithm employed. The IE formulation, originally proposed by Després [17] and later improved [18], is presented in Section III. Its main advantage resides in the fact that only Hermitian positive definite matrices need to be inverted. A few numerical results display its efficiency for the particular case of scattering by a nonpenetrable object. Section IV outlines the implementation of the FE–IE DDM algorithm. The numerical results obtained for the scattering from various inhomogeneous objects are presented in Section V that illustrate the potential of this technique, whose main advantages and drawbacks are summarized in Section VI.

II. STATEMENT OF THE PROBLEM AND DDM ALGORITHM

A monochromatic incident plane wave (E^{inc}, H^{inc}) illuminates the inhomogeneous body immersed in free-space. E and H designate the electric and magnetic fields, respectively.

Here, and in the following, $\underline{H}$ stands for $\eta_0 \underline{H}$, where η_0 is the free-space impedance. The assumed (and suppressed) time dependence is $\exp(i\omega t)$, and $k = 2\pi/\lambda = \omega/c$ is the wave number of the incident field (c is the light velocity). Without loss of generality, the Leontovich impedance boundary condition (LIBC) is prescribed upon the surface S_0 of the scatterer which may be coated by inhomogeneous materials of relative dielectric permittivity ϵ and magnetic permeability μ that are position dependent 3×3 tensors. To alleviate the notations, the dependence of all quantities on the coordinates is generally suppressed. We consider the solution of the following exact scattering problem. Find $\underline{E}$ and $\underline{H}$ that satisfy, in the unbounded domain exterior to S_0, the following set of equations:

$$\underline{\nabla} \times [\epsilon^{-1}\underline{\nabla} \times \underline{H}] - k^2 \mu \underline{H} = 0, \quad \underline{\nabla} \cdot (\mu \underline{H}) = 0, \quad \underline{E} = -\frac{i}{k}\epsilon^{-1}\underline{\nabla} \times \underline{H} \tag{2.1a}$$

$$\underline{n} \times \epsilon^{-1}\underline{\nabla} \times \underline{H} = -ikZ\underline{H}_{tg} \quad \text{on } S_0 \tag{2.1b}$$

$$\underline{H} = \underline{H}^{inc} + \underline{H}^{s}, \quad \underline{E} = \underline{E}^{inc} + \underline{E}^{s} \tag{2.1c}$$

$$\begin{aligned} r \to \infty : \underline{H}^{s}(r, \theta, \phi) &\sim -\frac{e^{-ikr}}{r}\underline{u}_r \times [\underline{u}_r \times \underline{H}^{0}(\theta, \phi)] \\ \underline{E}^{s}(r, \theta, \phi) &\sim -\frac{e^{-ikr}}{r}\underline{u}_r \times \underline{H}^{0}(\theta, \phi). \end{aligned} \tag{2.1d}$$

$\underline{n}$ designates the outward normal to S_0 as well as to all the surfaces that are considered in the following; (2.1b) is the LIBC, where Z is the normalized impedance prescribed on S_0 and $\underline{H}_{tg} = -\underline{n} \times (\underline{n} \times \underline{H}) \cdot (r, \theta, \phi)$ are the usual spherical coordinates and $\underline{u}_r$ is the unit radial vector in this coordinate system.

Now, we recall the DDM algorithm as formulated in [14, 15]. Ω is the computational domain ($\partial\Omega = S_0 \cup S$) that includes all the inhomogeneous materials and is partitioned into N concentric subdomains Ω_i, $1 \leq i \leq N$. S_{i-1} and S_i denote, respectively, the inner and outer boundaries of Ω_i, and $S = S_N$ (see Fig. 1). Let $\underline{E}_i^{\ell}$, $\underline{H}_i^{\ell}$ be the values of the fields

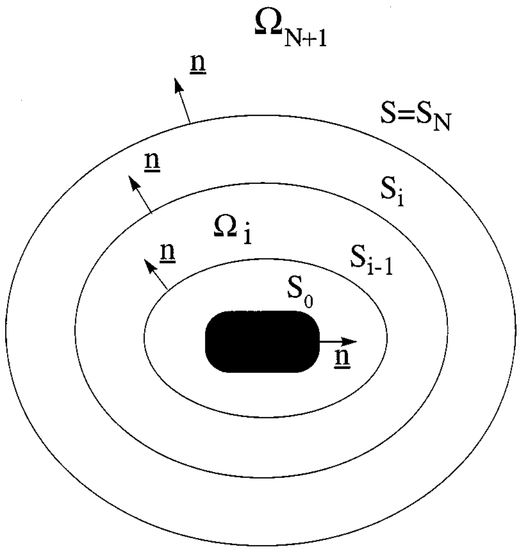

FIG. 1. "Onion-like" partitioning of the computational domain Ω.

in Ω_i at iteration ℓ. They satify Maxwell's equations in Ω_i

$$\nabla \times \left[\epsilon^{-1}\nabla \times \underline{H}_i^\ell\right] - k^2\mu \underline{H}_i^\ell = 0, \quad \nabla \cdot \left(\mu \underline{H}_i^\ell\right) = 0, \quad \underline{E}_i^\ell = -\frac{i}{k}\epsilon^{-1}\nabla \times \underline{H}_i^\ell \tag{2.2}$$

and the following zeroth order TCs on $\partial\Omega_i = S_{i-1} \cup S_i$

$$T^-\underline{H}_i^\ell = T^-\underline{H}_{i-1}^\ell \quad TC \;\text{ on } S_{i-1} \tag{2.3a}$$

$$T^+\underline{H}_i^\ell = T^+\left[\alpha_\ell \underline{H}_i^{\ell-1} + (1-\alpha_\ell)\underline{H}_{i+1}^{\ell-1}\right] \; TC \;\text{ on } S_i \tag{2.3b}$$

with $\alpha_1 = 0$, $0 \le \alpha_\ell \le 1/2$ for $\ell \ge 2$, and

$$T^\pm \underline{H} = \pm ik\underline{n} \times \underline{E} - ik\underline{H}_{tg} = \pm\underline{n} \times [\epsilon^{-1}\nabla \times \underline{H}] - ik\underline{H}_{tg} \tag{2.4}$$

ϵ and μ may be discontinuous on the interfaces. For $i = 1$, the LIBC (2.1b) is substituted to the TC on S_0:

$$\underline{n} \times \epsilon^{-1}\nabla \times \underline{H}_1^\ell = -ikZ\underline{H}_{1tg}^\ell \quad LIBC \;\text{ on } S_0. \tag{2.5}$$

The infinite free-space domain $R^3\backslash\Omega$ is considered as an additional subdomain Ω_{N+1}, and $(\underline{E}_{N+1}^\ell, \underline{H}_{N+1}^\ell)$ denote the fields in Ω_{N+1}. If

$$\begin{aligned} \underline{E}_{N+1}^{s\ell} &= \underline{E}_{N+1}^\ell - \underline{E}^{inc} \\ \underline{H}_{N+1}^{s\ell} &= \underline{H}_{N+1}^\ell - \underline{H}^{inc} \end{aligned} \tag{2.6}$$

then $(\underline{E}_{N+1}^{s\ell}, \underline{H}_{N+1}^{s\ell})$ satisfy Eqs. (2.1a), (2.1d) for all ℓ, with $\epsilon = \mu = 1$. $(\underline{E}_{N+1}^{s\ell}, \underline{H}_{N+1}^{s\ell})$ are connected to the fields in Ω_N by (2.3b), where $i = N$, and (2.3a), where $i = N+1$ which reads

$$T^-\underline{H}_{N+1}^\ell = T^-\underline{H}_N^\ell. \tag{2.7}$$

In fact, (2.7) is an inhomogeneous LIBC on S with $Z = 1$

$$-\underline{n} \times \underline{E}_{N+1}^{s\ell} - \underline{H}_{(N+1)tg}^{s\ell} = \underline{q}^\ell = \underline{n} \times \underline{E}^{inc} + \underline{H}_{tg}^{inc} - \underline{n} \times \underline{E}_N^\ell - \underline{H}_{Ntg}^\ell \tag{2.8}$$

and constitutes the boundary condition on S at iteration ℓ for the IE, defined in Section III, that relates the values on S of $\underline{n} \times \underline{E}_{N+1}^{s\ell}$ to those of $\underline{n} \times \underline{H}_{N+1}^{s\ell}$. If the solutions of this IE are unique and $Im\epsilon \le 0$, $Im\mu \le 0$ in Ω, then $\lim_{\ell\to\infty}(\underline{E}_i^\ell, \underline{H}_i^\ell) = (\underline{E}_{ex}, \underline{H}_{ex})$ in Ω_i, $1 \le i \le N+1$, where $(\underline{E}_{ex}, \underline{H}_{ex})$ denote the solutions of the original problem (2.1a–d) [15]. The initial values are chosen to be

$$\underline{H}_i^{\ell=0} = \underline{H}^{inc} \quad 1 \le i \le N \tag{2.9}$$

and we emphasize that the uniqueness and convergence of the DDM algorithm do not depend on this particular choice. For each value of ℓ, the problems P_i^ℓ, that correspond to Eqs. (2.2)–(2.8) and to the IE for $i = N+1$, are solved successively for increasing values of i.

III. INTEGRAL EQUATION FORMULATION

In view of the boundary condition (2.8) satisfied by the IE on S, we have implemented the IE formulation corresponding to the penalized system (with the β parameter) proposed in [18], and outlined in Section III.1 for the DDM. Since this formulation is new and has never been tested for 3-D problems, we investigate in Section III.2 its numerical efficiency for the particular case of scattering from a nonpenetrable object of surface S on which the LIBC (2.1b) is prescribed with $Z = 1$.

III.1. *IE Formulation for the DDM*

The IE is constituted by the two following, uncoupled, $+$ and $-$ systems:

$$\begin{pmatrix} \frac{1-\beta}{2} I + \frac{D_\pm}{4k^2} & k(K_\pm \pm i\beta I) \\ -k\left(K_\pm^H \mp i\beta I\right) & 2k^2\beta I + D_\pm \end{pmatrix} \begin{pmatrix} X_\pm^\ell \\ X_\pm^{\prime\ell} \end{pmatrix} = \begin{pmatrix} g_\pm^\ell \\ 0 \end{pmatrix}. \tag{3.1}$$

I is the identity operator, K^H designates the adjoint operator of K and

$$\begin{aligned} X_\pm^\ell &= \left(\underline{E}_{N+1}^{s\ell} \pm i\underline{H}_{N+1}^{s\ell}\right) \times \underline{n} \\ g_\pm^\ell &= (\underline{q}^\ell \mp i\underline{q}^\ell \times \underline{n})/2. \end{aligned} \tag{3.2}$$

Let Φ, $\tilde{\Phi}$ be tangential vectors to S and $(\underline{x}, \underline{y})$, $(x, y)_\infty$ designate the following Hermitian inner products

$$(\underline{x}, \underline{y}) = \int_S \underline{x}^*(\underline{r}) \cdot \underline{y}(\underline{r})\, d\underline{r}, \quad (x, y)_\infty = \int_0^\pi \sin\theta\, d\theta \int_0^{2\pi} x^*(\theta, \varphi) y(\theta, \varphi)\, d\varphi,$$

where x^* designates the complex conjuguate of x. The matrix elements of the operators $K_\pm$ and $D_\pm$, defined in Appendix A, are given by

$$\begin{aligned} (\tilde{\Phi}^*, K_\pm\Phi) = {} & -\int_{S\times S} \tilde{\Phi}(\underline{r}) \cdot [\Phi(\underline{r}') \times \nabla_r g_r(\underline{r}, \underline{r}')]\, d\underline{r}\, d\underline{r}' - \frac{1}{2}\int_S \tilde{\Phi}(\underline{r}) \cdot [\underline{n}(\underline{r}) \times \Phi(\underline{r})]\, d\underline{r} \\ & \mp k \int_{S\times S} \tilde{\Phi}(\underline{r}) \cdot \Phi(\underline{r}') g_r(\underline{r}, \underline{r}')\, d\underline{r}\, d\underline{r}' \\ & \pm \frac{1}{k}\int_{S\times S} [\nabla_{tg} \cdot \tilde{\Phi}(\underline{r})][\nabla'_{tg} \cdot \tilde{\Phi}(\underline{r}')] g_r(\underline{r}, \underline{r}')\, d\underline{r}\, d\underline{r}' \end{aligned} \tag{3.3a}$$

$$\begin{aligned} (\tilde{\Phi}^*, D_\pm\Phi) &= (\tilde{\Phi}^*, \delta_\pm^H \delta_\pm \Phi)_\infty \\ (\delta_\pm\Phi)(\theta, \varphi) &= \frac{k^2}{2\pi\sqrt{2}} \int_S \Phi(\underline{r}) \cdot \{[(\underline{u}_\theta \pm i\underline{u}_\varphi)\underline{n}(\underline{r})] \times \underline{n}(\underline{r})\} e^{-ik\underline{r}\cdot\underline{u}_r}\, d\underline{r} \\ \underline{u}_\theta &= (\cos\theta\cos\varphi, \cos\theta\sin\varphi, -\sin\theta)^t, \quad \underline{u}_\varphi = (-\sin\varphi, \cos\varphi, 0)^t \end{aligned} \tag{3.3b}$$

($\underline{u}^t$ designates the transpose of $\underline{u}$) with

$$g_r(\underline{r}, \underline{r}') = \frac{\cos(k|\underline{r} - \underline{r}'|)}{4\pi|\underline{r} - \underline{r}'|}, \quad g_i(\underline{r}, \underline{r}') = \frac{\sin(k|\underline{r} - \underline{r}'|)}{4\pi|\underline{r} - \underline{r}'|}.$$

The solutions $X_\pm^\ell$, $X_\pm^{'\ell}$ of systems (3.1) are unique if $0 < \beta < 1$. Besides, we have

$$X_\pm^{'\ell} = \mp\frac{i}{2k}X_\pm^\ell. \tag{3.4}$$

It is important to note that (3.4) holds for the exact, nondiscretized, system (3.1) only. In this case, the equations corresponding to the second line of (3.1) are equivalent to the EFIE and MFIE obtained on S when taking the limit from the interior of S, while those corresponding to the first line of (3.1) result from the incorporation of these IE in the LIBC (2.8).

III.2. *Scattering from S with the LIBC* (2.1*b*) *and* $Z = 1$

In this section, we solve

$$\begin{pmatrix} \frac{1-\beta}{2}I + \frac{D_\pm}{4k^2} & k(K_\pm \pm i\beta I) \\ -k\left(K_\pm^H \mp i\beta I\right) & 2k^2\beta I + D_\pm \end{pmatrix} \begin{pmatrix} X_\pm \\ X'_\pm \end{pmatrix} = \begin{pmatrix} g_\pm \\ 0 \end{pmatrix} \tag{3.5}$$

with

$$X_\pm = (\underline{E}^s \pm i\underline{H}^s) \times \underline{n} \tag{3.6a}$$

$$g_\pm = (\underline{q} \mp i\underline{q} \times \underline{n})/2, \quad \underline{q} = \underline{n} \times (\underline{E}^{inc} - \underline{n} \times \underline{H}^{inc}). \tag{3.6b}$$

The numerical implementation is as follows. S is meshed with triangles and $X_\pm$, $X'_\pm$ are represented by the standard H(div) edge basis functions [19]. In (3.3a, b), test and basis functions are identical: $\tilde{\underline{\Phi}} = \underline{\Phi}$. The matrix elements of $K_\pm$ are evaluated using a standard quadrature rule for nonadjacent triangles, and special care is taken for the integration of the singularity in $g_r(\underline{r}, \underline{r}')$ [20]. Regarding $D_\pm$, the integration on the unit sphere in $(\tilde{\underline{\Phi}}^*, \delta_\pm^H\delta_\pm\underline{\Phi})_\infty$ (see (3.3b)) is carried out by a Gauss–Legendre quadrature rule. Following [17], (3.5) is solved by first computing $X'_\pm$, which yields

$$\begin{gathered} \{k^2(K_\pm^H \mp i\beta I)A^{-1}(K_\pm \pm i\beta I) + 2k^2\beta I + D_\pm\}X'_\pm = k(K_\pm^H \mp i\beta I)A^{-1}g_\pm \\ X_\pm = A^{-1}[g_\pm - k(K_\pm \pm i\beta I)X'_\pm] \\ A = \frac{1-\beta}{2}I + \frac{D_\pm}{4k^2}. \end{gathered} \tag{3.7}$$

The main advantage of this formulation resides in the fact that all the matrices that need to be inverted, namely $[k^2(K_\pm^H \mp i\beta I)A^{-1}(K_\pm \pm i\beta I) + 2k^2\beta I + D_\pm]$ and A, are Hermitian positive definite (if $0 < \beta < 1$). As a consequence, (3.7) can be solved by using a very simple double CG: A first one (CG1) to invert A—in fact $Ax = b$ is solved, with A preconditioned by the diagonal—and a second one (CG2) for the solution of (3.7) with no preconditioning. Note that $Ax = b$ must be solved twice for each iteration of the CG2. Besides, since systems $+$ and $-$ are uncoupled, they can be solved successively. First, matrices $D_\pm$ and $\tilde{K}_\pm$—obtained from $K_\pm$ by omitting the single integral term in (3.3a) which is recalculated at each iteration—are real symmetric and computed and stored on out-of-core binary files. Then, $\tilde{K}_+$ and D_+ are read on these files, system $+$ is solved, and the procedure is repeated for system $-$. As a result, the memory required for the solution of (3.5) corresponds to the storage of $\tilde{K}_+$ and D_+ (or $\tilde{K}_-$ and D_-), i.e., to the storage of $N_S(N_S + 1)$ real numbers, N_S being the number of edges on S. The CG1 is stopped at iteration n satisfying

$$\text{CG1} : \|(Ax^n - b)/b\| \leq r_1 \tag{3.8}$$

($\|\cdot\|$ is the L^2 norm). For the exact solutions of system (3.5), we have the equivalent of (3.4), namely,

$$X'_{\pm} = \mp \frac{i}{2k} X_{\pm}. \tag{3.9}$$

Let us define the discrepancy, due to discretization, between the l.h.s. and r.h.s. in (3.9) at iteration n of the CG2 by

$$\Delta^n_{\pm} = \|X^n_{\pm} \mp 2ikX'^n_{\pm}\|. \tag{3.10}$$

For reasons that will be explained in the following, the CG2 is stopped when

$$\text{CG2} : \left|1 - \frac{\Delta^n_{\pm}}{\Delta^{n-1}_{\pm}}\right| \leq r_2 \tag{3.11}$$

We have verified, through various numerical experiments, that the value of β ($0 < \beta < 1$) has little incidence on the results, and all the calculations presented in this paper have been carried out with $\beta = 0.25$. The first numerical experiments have been performed at 300 MHz on a sphere of radius 30 cm. If $\underline{z}$ is directed along an axis of the sphere, the incident field is given by

$$\begin{aligned}
\underline{E}^{inc}(x, y, z) &= \underline{V}_1 \exp i\chi(x, y, z), \quad \underline{H}^{inc}(x, y, z) = \underline{V}_2 \exp i\chi(x, y, z) \\
\chi(x, y, z) &= k(x \sin\theta^{inc} \cos\varphi^{inc} + y \sin\theta^{inc} \sin\varphi^{inc} + z \cos\theta^{inc}) \\
\underline{V}_1 &= (\cos\theta^{inc} \cos\varphi^{inc}, \cos\theta^{inc} \sin\varphi^{inc}, -\sin\theta^{inc})^t \\
\underline{V}_2 &= (\sin\varphi^{inc}, -\cos\varphi^{inc}, 0)^t
\end{aligned} \tag{3.12a}$$

for TM polarization and, for TE polarization,

$$\underline{E}^{inc}(x, y, z) = \underline{V}_2 \exp i\chi(x, y, z), \quad \underline{H}^{inc}(x, y, z) = -\underline{V}_1 \exp i\chi(x, y, z). \tag{3.12b}$$

On Fig. 2 is plotted the bistatic RCS vs the angle of observation θ with $\varphi = 0$ ($\theta^{inc} = \varphi^{inc} = 0$)

$$\text{RCS}(\theta) = 10 \log\left[\lim_{r\to\infty} 4\pi r^2 |\underline{E}^s(r, \theta, \varphi = 0)|^2\right]$$

computed from the Mie series (exact RCS), the values of $X_{\pm}$ on S (RCS) and those of $X'_{\pm}$ (RCS$'$) for two values of r_1, r_2. Notice that RCS and RCS$'$ are polarization independent since system (3.5) is invariant under the transformation $W : (\underline{E}^s, \underline{H}^s) \mapsto (-\underline{H}^s, \underline{E}^s)$. The RCSs computed from (3.5) are in excellent agreement with the exact one: $N_S = 1638$, and the average length of the edges, $\overline{\ell^{edge}_S}$, is $\lambda/20$. Also, Fig. 2 plots r_{CG2}

$$r_{\text{CG2}} = \|Cx^n - b\|,$$

where C and b represent, respectively, the matrix and the r.h.s. of the first equation in (3.7), and Δ^n_- vs the number n of CG2 iterations (both $+$ and $-$ systems behave very similarly). We observe that Δ^n_- reaches a plateau that corresponds to the discretization error (see Appendix A). Decreasing r_1 and r_2 does not change the value of Δ^n_-: this is the

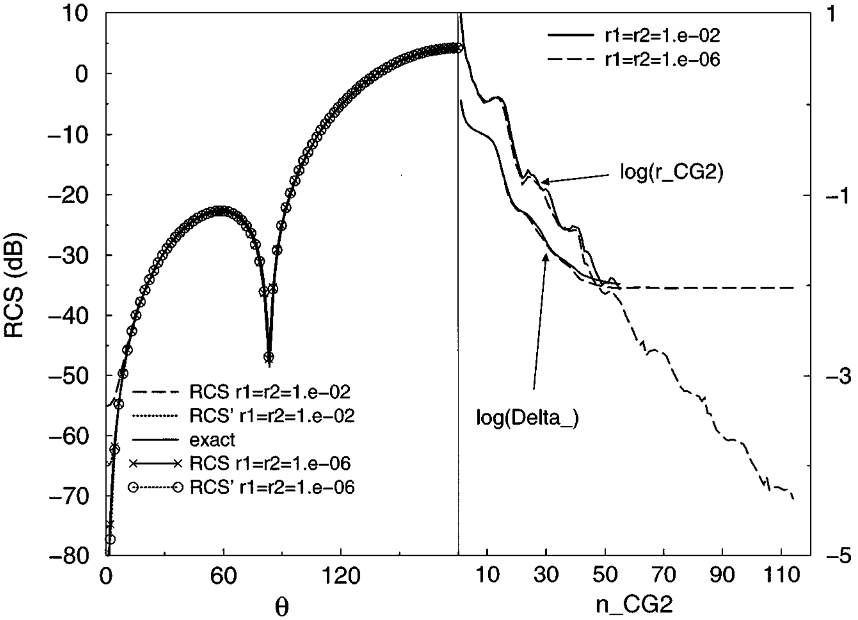

FIG. 2. Sphere with $Z = 1$. IE formulation with $\theta^{inc} = 0$. Left: RCS vs the angle of observation θ. Right: r_{CG2} and Δ_{-}^{n} vs the number of CG2 iterations.

reason we have chosen (3.11) as the stop criterion for the CG2, rather than the residual error r_{CG2}. However, it does increase the RCS accuracy in the vicinity of $\theta = 0$ (see Fig. 2). This observation, in apparent contradiction with the previous statement, comes from the fact that the backscattered far-field is identically zero for an object with $Z = 1$, illuminated in axial incidence and invariant by a rotation of $\pi/4$ around the axis [21]. Since (3.5) is invariant under the transformation W, $\mathrm{RCS}(\theta = 0) = -\infty$ for the solutions of (3.5) obtained when $r_1 = r_2 = 0$ if the mesh of the sphere has the proper symmetry, independently of the discretization error. Similar comments can be made regarding the results obtained at 500 MHz on the cone-sphere corresponding to surface S_1 in Fig. 5—total length 2.2 m, back-sphere radius 0.4 m, round tip radius 0.1 m, and $N_S = 13179$ ($\overline{\ell_S^{edge}} = \lambda/20$)—in axial, on tip incidence ($\theta^{inc} = \varphi^{inc} = \varphi = 0$): see Fig. 3 that plots also the reference RCS computed with a MoM code for bodies of revolution (BORs) [22] (the exact RCS is polarization independent). The plots of r_{CG2} and Δ_{-}^{n} vs n for both the cone sphere and the former sphere at 300 MHz displayed in Fig. 3 show that the plateau of Δ_{-}^{n} and the number of CG2 iterations are similar for both geometries. The same conclusion holds true for the CG1: the number of CG1 iterations required to solve one of the two systems $Ax = b$ for a given CG2 iteration number comprises between 3 and 4. Calculations performed at various frequencies on the same meshes have confirmed that, for fixed values of r_1 and r_2, the minimum of $\Delta_{\pm}^{n}$, as well as the number of CG2 iterations, depend on $\overline{\ell_S^{edge}}$ rather than on the shape of S, while the number of CG1 iterations remains fairly constant. $\Delta_{\pm}^{n}$ decreases and the number of CG2 iterations increases when the calculation frequency decreases. An important and, as far as we know, unique feature of this IE formulation is that the value of the plateau reached by $\Delta_{\pm}^{n}$ constitutes an indicator of the accuracy with which the problem has been solved.

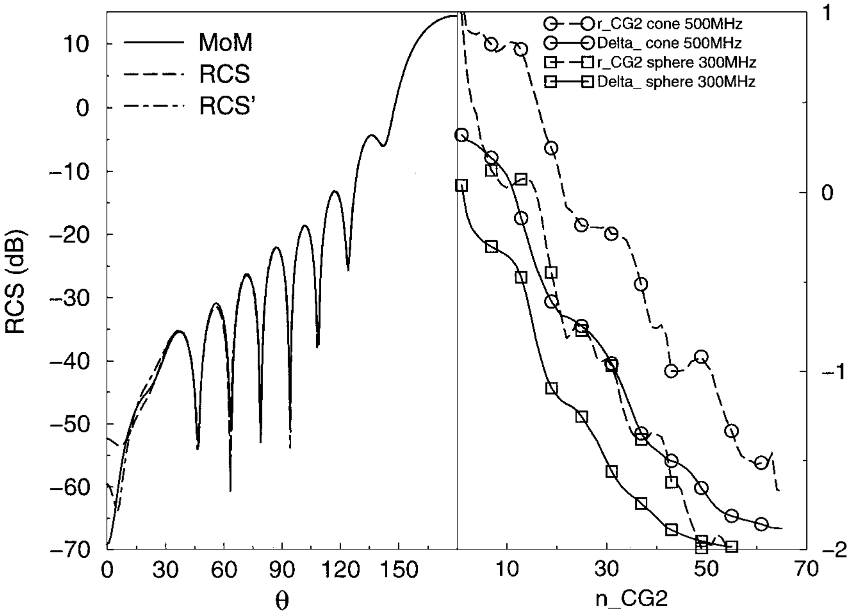

FIG. 3. Cone-sphere with $Z = 1$. IE formulation with $\theta^{inc} = 0$. Left: RCS vs θ. Right: r_{CG2} and Δ^n_- vs the number of CG2 iterations for the cone-sphere and the sphere of Fig. 2.

IV. IMPLEMENTATION OF THE FE–IE DDM ALGORITHM

Regarding the FE region ($1 \leq i \leq N$), we proceed exactly as in [14]: Each subdomain Ω_i is meshed with tetrahedrons, first-order edge-basis functions are employed and a Galerkin procedure is used. The basis functions are compatible with those used on S for the IE ($\underline{\Phi} = \underline{n} \times \underline{h}$ if $\underline{h}$ designates a FE basis function). Then, we solve successively the following systems

$$A_i H_i^\ell = b_i^\ell \tag{4.1a}$$

that result from the discretization of the variational formulation

$$\begin{aligned} &\int_{\Omega_i} \left\{ (\underline{\nabla} \times \tilde{\underline{H}}) \cdot \epsilon^{-1} \left(\underline{\nabla} \times \underline{H}_i^\ell \right) - k_0^2 \tilde{\underline{H}} \cdot \mu \underline{H}_i^\ell \right\} d\Omega + ik \int_{S_{i-1}} \tilde{\underline{H}}_{tg} \cdot \underline{H}_{itg}^\ell \, dS \\ &\quad + ik \int_{S_i} \tilde{\underline{H}}_{tg} \cdot \underline{H}_{itg}^\ell \, dS = b_i^\ell \end{aligned} \tag{4.1b}$$

(A_i is symmetric) with

$$\begin{aligned} &i = 1 : b_1^1 = -\int_{S_1} \tilde{\underline{H}}_{tg} \cdot T^+ \underline{H}^{inc} \, dS \\ &\ell \geq 2 : b_1^\ell = b_1^{\ell-1} + 2ik(1 - \alpha_\ell) \int_{S_1} \tilde{\underline{H}}_{tg} \cdot \left(\underline{H}_{2tg}^{\ell-1} - \underline{H}_{1tg}^{\ell-1} \right) dS. \end{aligned} \tag{4.2a}$$

$$\begin{aligned} 2 \leq i \leq N : b_i^1 = &-\int_{S_i} \tilde{\underline{H}}_{tg} \cdot T^+ \underline{H}^{inc} \, dS + \int_{S_i - 1} \tilde{\underline{H}}_{tg} \cdot T^+ \underline{H}^{inc} dS \\ &+ 2ik \int_{S_i - 1} \tilde{\underline{H}}_{tg} \cdot \underline{H}_{(i-1)tg}^1 dS \end{aligned}$$

$$\begin{aligned}\ell \geq 2 : b_i^{\ell} &= b_i^{\ell-1} + 2ik(1-\alpha_\ell)\int_{S_i} \tilde{\underline{H}}_{tg}\cdot\left(\underline{H}^{\ell-1}_{(i+1)tg} - \underline{H}^{\ell-1}_{itg}\right) dS \\ &\quad + 2ik\int_{S_i-1} \tilde{\underline{H}}_{tg}\cdot\left[\underline{H}^{\ell}_{(i-1)tg} - \underline{H}^{\ell-1}_{itg} + \alpha_\ell\left(\underline{H}^{\ell-1}_{itg} - \underline{H}^{\ell-1}_{(i-1)tg}\right)\right] dS. \qquad (4.2b)\end{aligned}$$

For the last subdomain ($i = N$), we compute $\underline{H}^{\ell-1}_{(N+1)tg}$ from the arithmetical mean of $X_\pm^{\ell-1}$ and $X_\pm^{\prime\ell-1}$ on account of (3.2) and (3.4)

$$\underline{H}^{\ell-1}_{(N+1)tg} = \underline{H}^{inc}_{tg} + \frac{i}{4}\underline{n}\times\left[X_-^{\ell-1} - 2ikX_-^{\prime\ell-1} - \left(X_+^{\ell-1} + 2ikX_+^{\prime\ell-1}\right)\right]. \qquad (4.3)$$

Regarding the IE in (3.1), the r.h.s. $g_\pm^\ell$ is computed recursively from its definition in (3.2) by using the TCs on S. We get

$$\ell = 1 : g_\pm^1 = \underline{H}^{inc} \mp i\underline{H}^{inc}\times\underline{n} - \left(\underline{H}^1_{Ntg} \mp i\underline{H}^1_N\times\underline{n}\right) \qquad (4.4a)$$

$$\begin{aligned}\ell \geq 2 : g_\pm^\ell &= g_\pm^{\ell-1} + (1-\alpha_\ell)(\underline{H}^{inc} \mp i\underline{H}^{inc}\times\underline{n}) - \left(\underline{H}^\ell_{Ntg} \mp i\underline{H}^\ell_N\times\underline{n}\right) \\ &\quad + \alpha_\ell\left(\underline{H}^{\ell-1}_{Ntg} \mp i\underline{H}^{\ell-1}_N\times\underline{n}\right) + \frac{1-\alpha_\ell}{2}\left[\mp\left(X_+^{\ell-1} - X_-^{\ell-1}\right)\right. \\ &\quad \left. - i\underline{n}\times\left(X_+^{\ell-1} - X_-^{\ell-1}\right)\right]. \qquad (4.4b)\end{aligned}$$

For each polarization TM or TE of the incident wave, and for a given value of ℓ, we proceed as follows:

- $1 \leq i \leq N$: Compute A_i and solve (4.1a) using a CG (the initial solution is $H_i^{\ell-1}$); stop the CG when

$$\left\|A_i H_i^\ell - b_i^\ell\right\| \leq \epsilon_{CG}. \qquad (4.5)$$

- $i = N+1$: Compute $\tilde{K}_\pm$, $D_\pm$ and write the values on out-of-core binary files (for $\ell = 1$ only). Read $\tilde{K}_-$, D_- and solve system $-$ of (3.1), read $\tilde{K}_+$, D_+ and solve system $+$ (the initial solutions for the CG2 are $X_\pm^{\ell-1}$, $X_\pm^{\prime\ell-1}$); the stop criteria of the CGs are those defined in Section III.2.

The DDM algorithm is stopped for the smallest value L of ℓ satisfying

$$\left\|H_1^{L+1} - H_1^L\right\| \leq 3\epsilon_{CG}. \qquad (4.6)$$

The IE systems in (3.1) are solved L times.

V. NUMERICAL RESULTS

The results that are presented in this section have been obtained on a sphere, a cone-sphere, a "stopper," and the air intake defined in [8] ("channel"). The first three objects are inhomogeneous BORs. No symmetry is taken into account, and fully 3-D meshes are used. For the sake of simplicity, ϵ and μ are scalar and assumed to be constant in each subdomain: ϵ_i and μ_i designate the values of ϵ and μ in Ω_i, $1 \leq i \leq N$. The relaxation parameter α_ℓ, as defined in Section II, is chosen at random at each iteration. All the RCSs that have been computed are bistatic with $\varphi^{inc} = \varphi = 0$. A hybrid FE–CFIE code for BORs [3] serves as a reference for the BORs and a 3-D MoM code [23] for the channel. The calculations are performed on one processor only of a Cray T90. Sections V.1 to V.4 are devoted to the results that have been obtained on each of these four objects.

V.1. *Sphere*

The radius of the sphere is 25 cm, and the subdomains are spherical shells: The radii of S_1, S_2, and $S_3 = S$ are 30, 34, and 37 cm, respectively. The calculation frequency is 300 MHz. $Z = 1$ in (2.5), $N = 3$, and $\epsilon_i = \mu_i$, $1 \le i \le 3$, with $\epsilon_1 = 2$, $\epsilon_2 = 0.71(1 - i)$, and $\epsilon_3 = (1 - i)/2$, so that the conditions of applition of Weston's theorem [21] are satisfied. Since the FE formulation (4.1b) is not invariant under the W transformation, *this particular choice of the parameters constitutes a severe test for numerical accuracy*. The RCS calculated with $r_1 = r_2 = \epsilon_{GC} = 10^{-6}$ is compared to the exact one computed with the Mie series on Fig. 4: the average length of the edges in all of the subdomains, $\overline{\ell_V^{edge}}$, is equal to $\lambda/20$, and $\overline{\ell_S^{edge}} = \lambda/20$. Also, we verify that the DDM does converge on Fig. 4 that plots

$$er_1(\ell) = \left\| H_1^{\ell} - H_1^{\ell-1} \right\|$$

vs the number ℓ of DDM iterations, ($L = 163$), and r_{CG2}, Δ_-^n for system $-$ of (3.1)—system $+$ behaves very similarly—vs the total number of CG2 iterations. Note that the last quantities show peaks for each new value of ℓ. Although not shown here, a calculation

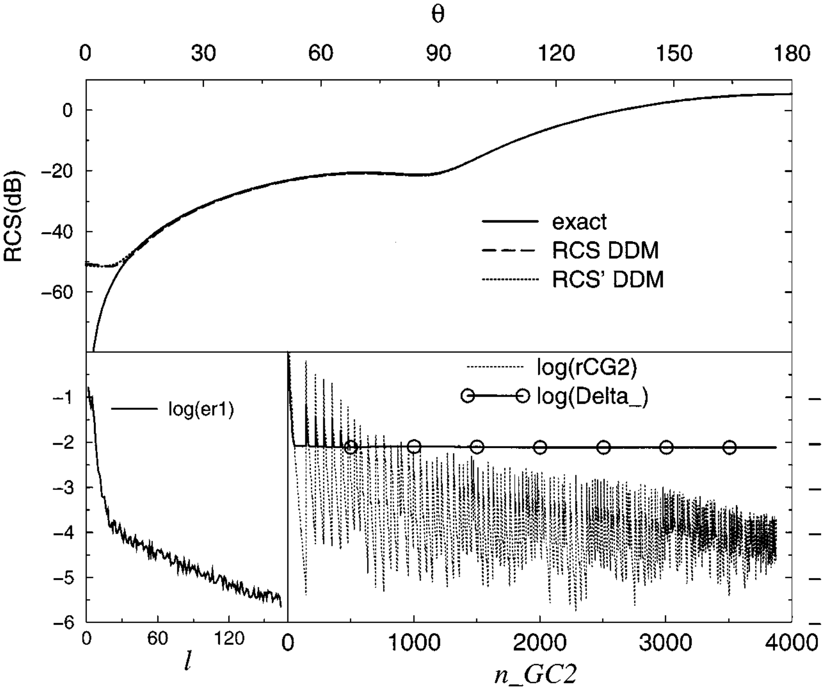

FIG. 4. Sphere with a three layer coating and $Z = 1$, $N = 3$. $\epsilon_i = \mu_i$, $1 \le i \le 3$, $\theta^{inc} = 0$, and $r_1 = r_2 = \epsilon_{GC} = 10^{-6}$. Top: RCS vs θ. Bottom: er_1 vs the number ℓ of DDM iterations and r_{CG2}, Δ_-^n vs the total number of CG2 iterations.

performed with $r_1 = r_2 = \epsilon_{GC} = 10^{-2}$ yields the same values for the RCS, but with a much smaller number of DDM iterations ($L = 6$).

V.2. *Cone-Sphere*

It is identical to the one defined in [14]: The total length of the object is 2 m, the radius of the sphere is 30 cm, and the tangent is continuous at the junction between the sphere and the cone (see sketch on Fig. 5). $N = 3$, the interfaces conform to S_0, and the distances d_i separating them are, for increasing values of i, 10, 8, and 6 cm, so that S is placed 24 cm away from S_0. The calculation frequency is 500 MHz, and the characteristics of the meshes are the following (N_i^{el} and N_i^{un} denote the number of elements and unknowns in subdomain Ω_i, respectively): $N_1^{el} = 75358$, $N_1^{un} = 98534$, $\overline{\ell}_V^{edge} = \lambda/22$; $N_2^{el} = 60437$, $N_2^{un} = 82337$, $\overline{\ell}_V^{edge} = \lambda/17$; $N_3^{el} = 25945$, $N_3^{un} = 39450$, $\overline{\ell}_V^{edge} = \lambda/13$; $N_S = 7950$, $\overline{\ell}_S^{edge} = \lambda/12$. $\underline{z}$ is the axis of the cone illuminated in axial, on tip, incidence ($\theta^{inc} = \varphi^{inc} = 0$).

The first results have been obtained with $Z = 0$—perfectly electric conducting (PEC) cone-sphere—$\epsilon_1 = 1.4(1 - i)$, $\mu_1 = 1$, $\epsilon_2 = 1 - i$, $\mu_2 = (1 - i)/2$, $\epsilon_3 = 2$, $\mu_3 = (1 - i)/4$, $\epsilon_{GC} = 10^{-2}$, $r_1 = 10^{-3}$, and $r_2 = 10^{-2}$. $L = 7$ and the ratio of the number of CG iterations—relative to the solution of the FE systems (4.1a)—to the number of unknowns comprises between 7.10^{-4} and 5.10^{-3}. The total number of CG2 iterations for one of the two systems in (3.1) is 92, with an average of 6 CG1 iterations per CG2 iteration. Once $D_\pm$, $\tilde{K}_\pm$ are computed, the total CPU time for one polarization is 4000 s, of which 1800 s for the FE systems (4.1a) (we recall that the A_i matrices are recomputed for each ℓ). As an indication, the total memory storage is 80 M words (double precision arithmetic is the standard on CRAY T90, so that 1 word $= 8$ bytes). The IE formulation alone requires $N_S^2 = 63$ M words. RCS, RCS′, and the reference RCS are plotted on Fig. 6 which also displays Δ_-^n, r_{CG2}, and $er_1(\ell)$.

On account of the widely admitted rule of thumb requiring that $\overline{\ell}_V^{edge} \simeq \lambda/(10|\nu|)$ for a given subdomain, where $\nu = \sqrt{\epsilon\mu}$ is the optical index of the medium, a large index implies a large value of N_S if S is the interface between the material and the surrounding free-space, and much larger computer resources are required for the solution of (3.1) than if S is located in free-space with $\overline{\ell}_S^{edge} \simeq \lambda/10$. Consequently, inserting one or several free-space subdomains allows a reduction of these resources. A computation performed at 500 MHz with $N = 3, Z = 1, \epsilon_1 = \mu_1 = 2, \epsilon_2 = \mu_2 = \epsilon_3 = \mu_3 = 1$, and $\epsilon_{GC} = r_1 = r_2 = 10^{-2}$ ($L = 11$, total number of CG2 iterations equal to 155 with an average of 4 CG1 iterations per CG2 iteration) shows that we get an accuracy for the RCS similar to the one achieved in the previous calculation (see Fig. 7). Compared with a computation performed with subdomain Ω_1 alone ($N = 1$), the memory storage is reduced by a factor 2.2, approximately equal to $(N_{S_1}/N_{S_3})^2 = (13179/7950)^2$, on account of the fact that the memory required to solve the

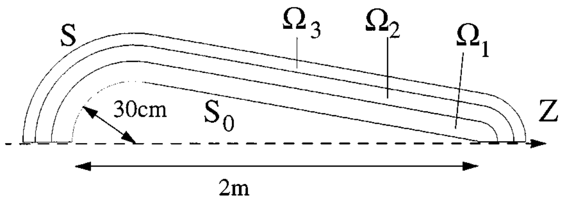

FIG. 5. Cone-sphere: Geometry and domain partitioning.

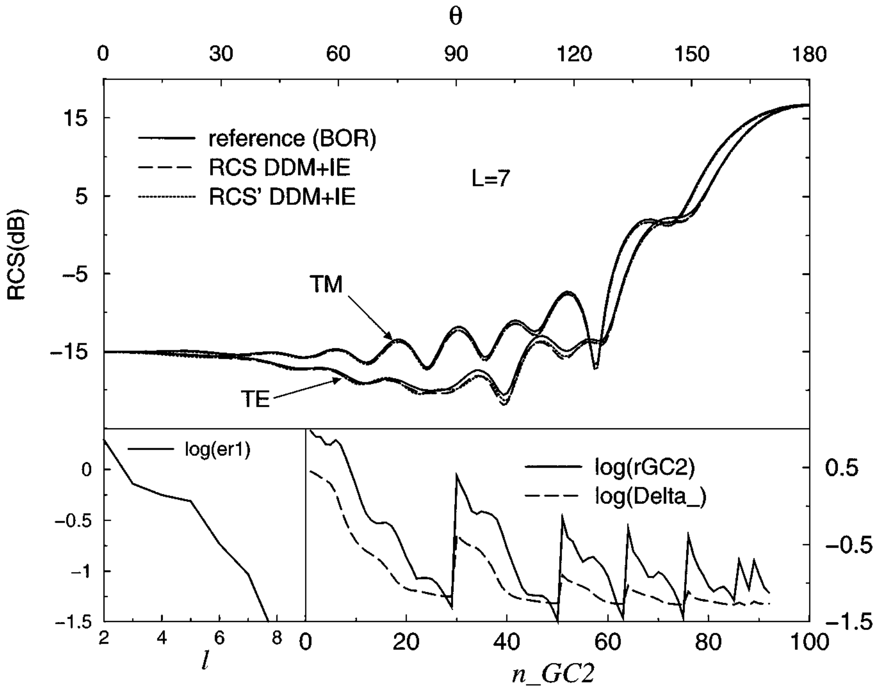

FIG. 6. Cone-sphere with a three layer coating and $Z = 0$, $N = 3$, $\theta^{inc} = 0$. Top: RCS vs θ. Bottom: er_1 vs the number ℓ of DDM iterations and r_{CG2}, Δ_{-}^{n} vs the total number of CG2 iterations.

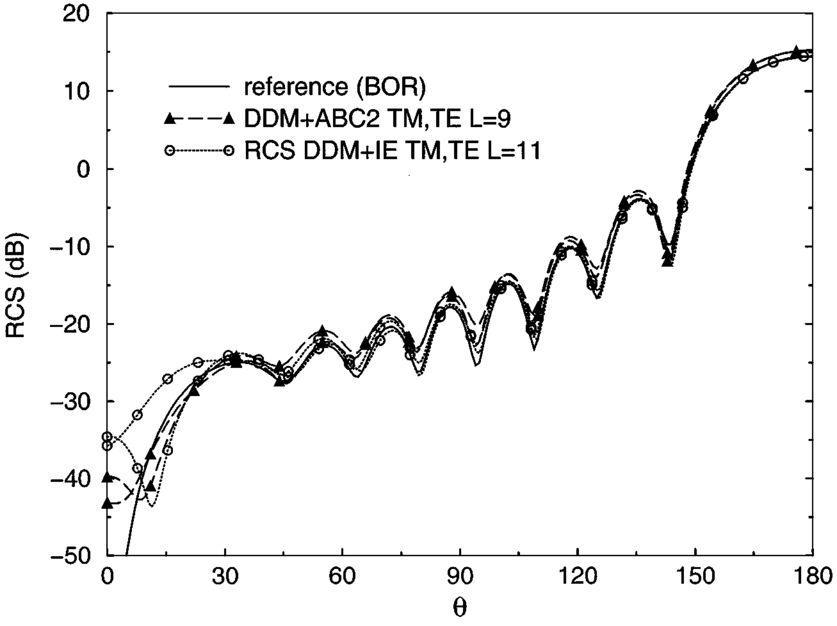

FIG. 7. Cone-sphere with a monolayer coating and $Z = 1$, $N = 3$, $\theta^{inc} = 0$. Free-space in $\Omega_2 \cup \Omega_3$. IE or ABC2 on S.

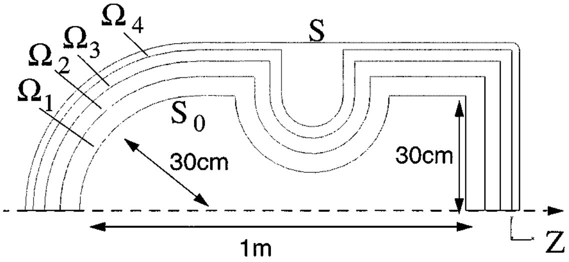

FIG. 8. Stopper: Geometry and domain partitioning.

largest of the FE systems in (4.1b) is small compared to the one required to solve the IE systems in (3.1). Another way to reduce the computational complexity is to implement on $S_3 = S$ the second-order conformal ABC [24] (termed ABC2) as in [14] with $N = 3$. We observe on Fig. 7 that the accuracy of the RCS thus computed ($L = 9$) is similar to the one achieved with the IE and the memory storage is divided by 8 and the CPU time by 3 (the distance between S_0 and S_3 is equal to $\lambda/2.5$).

V.3. *Stopper*

Stopper is sketched on Fig. 8: total length 1 m, radius of the hemisphere 30 cm. Four subdomains are used. S_1, S_2, S_3 are partially concave and present sharp edges. Because we will also implement the ABC2 on $S = S_4$, S has a bevelled edge. One of the reasons that has motivated the calculations presented in this section was to verify that partially concave interfaces with singularities had no impact on the behavior of the algorithm, as it has already been done in [13] for the 2-D case. The distances d_i separating the interfaces are, for increasing values of i, 5, 4, 3, and 2 cm. The characteristics of the meshes are the following: $N_1^{el} = 59753$, $N_1^{un} = 82277$, $\overline{\ell}_V^{edge} = \lambda/25$; $N_2^{el} = 22367$, $N_2^{un} = 35383$, $\overline{\ell}_V^{edge} = \lambda/17$; $N_3^{el} = 14465$, $N_3^{un} = 23995$, $\overline{\ell}_V^{edge} = \lambda/17$; $N_4^{el} = 16638$, $N_4^{un} = 26089$, $\overline{\ell}_V^{edge} = \lambda/13$; $N_S = 6171$, $\overline{\ell}_S^{edge} = \lambda/13$. The computational frequency is 500 MHz, $Z = 1$, $\epsilon_{GC} = r_1 = r_2 = 10^{-2}$, and $\epsilon_i = \mu_i$, $1 \leq i \leq N = 4$.

The first results have been obtained with $\epsilon_1 = 1 - i$, $\epsilon_2 = 2$, $\epsilon_3 = 0.71(1 - i)$, and $\epsilon_4 = (1 - i)/2$. Figure 9a plots the RCS computed in normal incidence on the cylindrical part ($\theta^{inc} = 90^0$): $L = 8$, and the total number of CG2 iterations for one IE system is 154. Despite the large dynamic range of the RCS, the DDM achieves a reasonable accuracy. Note that the exact RCS is polarization independent. This is verified by the FE–CFIE formulation for BORs used as a reference since it is invariant under the W transformation, contrary to the DDM formulation. Another calculation is performed under the same incidence with $\epsilon_1 = 0.71(1 - i)$, $\epsilon_2 = \epsilon_3 = \epsilon_4 = 1$ (see Fig. 9b): $L = 12$ and the total number of CG2 iterations for one IE system is equal to 263. Also, are plotted on Fig. 9b the RCSs computed with $N = 4$ and the ABC2 on S. We observe that the IE provides a noticeable increase of the accuracy. Note that the distance ($\lambda/6.7$) between S and S_0 is small for the ABC.

V.4. *Air Intake ("Channel")*

The geometry is an evolutive channel enclosed in a circular cylinder of axis z, length 1.365 m, and radius 0.147 m. The entry of the channel has an elliptic cross-section, and the closed end has a circular cross-section (see Fig. 10). We refer to [8] for additional

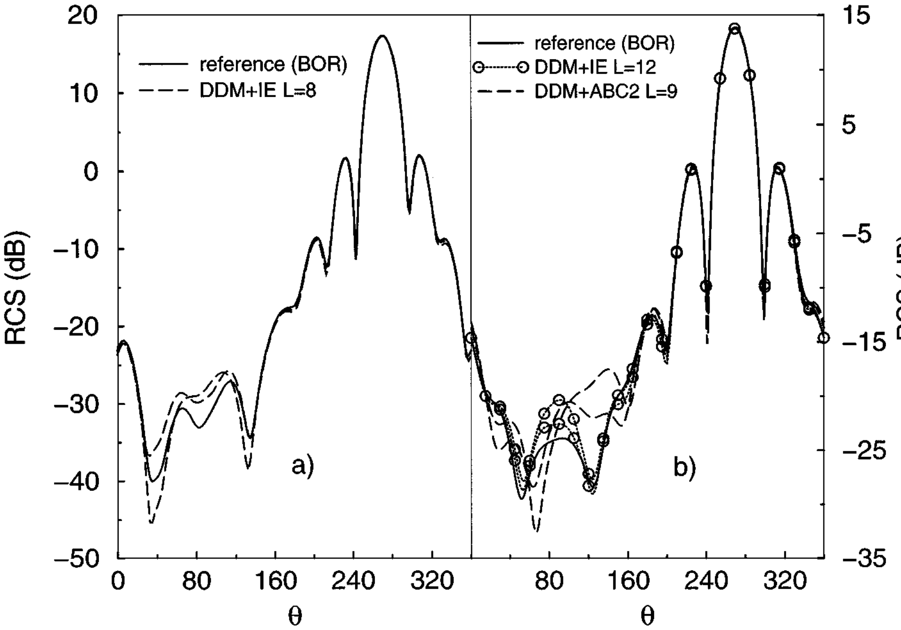

FIG. 9. Stopper with $Z = 1$, $N = 4$, $\epsilon_i = \mu_i$, $1 \leq i \leq 4$, and $\theta^{inc} = 90^0$. Left: Four layers coating and IE on S. Right: Monolayer coating and free-space in $\Omega_2 \cup \Omega_3 \cup \Omega_4$. IE or ABC2 on S.

information on the geometry (note that the definition of the x, y, z axes differs from the one in [8]). The object is perfectly conducting ($Z = 0$). The wave is obliquely incident on the entry of the channel with $\theta^{inc} = 30^0$, and the computational frequency is 1.1 GHz.

To minimize N_S, we have enclosed the channel in a cylinder of axis z whose surface S_1 is placed as close as possible to the exterior surface of the object: The distance between S_0 and S_1 is 5 mm (see Fig. 10). $N = 1$ ($S_1 = S$) and the length of the edges in the volume mesh of Ω_1, constituted of free-space, varies from $\lambda/15$ on S_0 to $\lambda/11$ on S_1: $N_1^{el} = 54899$, $N_1^{un} = 80592$, $N_S = 8682$, and the memory storage is 84 M words. The RCS is computed from the DDM + IE with $\epsilon_{GC} = r_1 = r_2 = 10^{-2}$ and a MoM code [23] using the EFIE

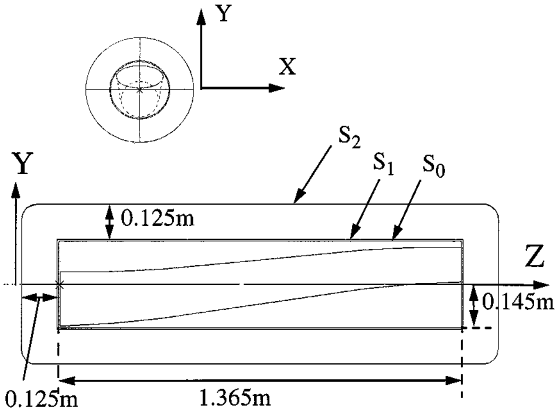

FIG. 10. Channel: Geometry and domain partitioning.

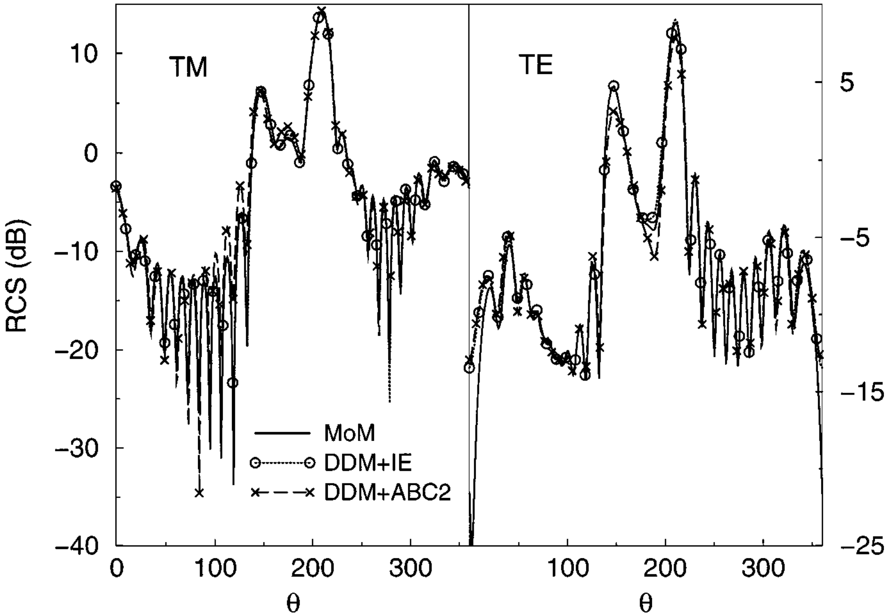

FIG. 11. Channel, $\theta^{inc} = 30^0$, $Z = 0$, and free-space in Ω_1. DDM + IE: N = 1 and IE on $S = S_1$. DDM + ABC2: N = 2 and free space in Ω_2; ABC2 on $S = S_2$.

on S_0 with the same surface mesh (24.087 edges) than in the volume mesh. Both are plotted on Fig. 11. In TM polarization, we observe that the MoM and DDM + IE results are superimposed while, in TE, they differ in the vicinity of the z axis ($\theta = 0^0$). We may explain this as follows. The first cavity mode is not excited in TM (E^{inc} is parallel to the major axis of the elliptical aperture). As a consequence, the field does not enter the channel and the air intake behaves essentially like a closed PEC cylinder. Conversely, this mode is excited in TE (E^{inc} is parallel to the minor axis of the ellipse), the field enters the channel and reradiates through the aperture. In this case, it is well known (see, e.g., [25]) that a high numerical accuracy is necessary to properly model the field propagation inside the duct, and low-order elements are used in the present FEM. A noticeable characteristic of the DDM calculation is the high value of L ($L = 18$). This may be due to the very small distance separating S and S_0: Like the ABC from which it is derived, the TC is all the more efficient as the surface on which it is implemented is situated far away from S_0 [13]. Also, the CG used to solve the FE system (4.1a) converges more slowly than in the previous cases, on account of the losseless cavity and $Z = 0$: The ratio of the number of CG iterations to the number of unknowns comprises between 3.10^{-3} and 5.10^{-2}. However, it is important to note that the solutions to the IE systems remain unaffected by the cavity: The total number of CG2 iterations for one of the two systems in (3.1) is 220, with an average of 4 CG1 iterations per CG2 iteration.

Then, we have added another subdomain Ω_2 (see Fig. 10) on the boundary S_2 of which is implemented the ABC2. S_2 is conform to S_1—except for the edges that have been rounded—and its distance from S_0 is equal to 0.125 m $= \lambda/2.2$; $N_2^{el} = 140317$, $N_2^{un} = 183322$, and $\overline{\ell}_V^{edge} = \lambda/13$. The RCSs computed with $N = 2$ ($S_2 = S$) and $\epsilon_{GC} = 10^{-2}$ ($L' = 16$) are also plotted on Fig. 11, and the accuracy achieved is reasonably good. Compared with the DDM + IE calculation, the memory storage and CPU time are divided by 4 and 1.4, respectively.

VI. CONCLUSIONS

We may consider that the numerical results presented in this paper validate the hybrid FE–IE DDM proposed in [15] for the scattering by inhomogeneous 3-D objects. The main advantages offered by this technique are the following.

(1) All the linear systems that are solved in the DDM algorithm possess unique solutions.
(2) These solutions converge to those of the original problem if $Im(\epsilon) \leq 0$, $Im(\mu) \leq 0$.
(3) Each of the FE and IE systems are solved separately, thus reducing the complexity of the original problem:

—Regarding the FE region, the interface between the subdomains may be located anywhere, may include concave parts, and may present surface singularities. The memory storage is $O(N^{el}_{max})$, and the convergence of the CG used to solve the FE systems is accelerated thanks to the lossy boundary conditions (TCs). As an example, a large problem involving more than $1.3 \cdot 10^6$ elements and $1.6 \cdot 10^6$ unknowns has been easily solved on one processor of a CRAY T90 with a storage of 53 M words [14].

—Regarding the particular IE formulation employed in this paper, all the matrices that are inverted are Hermitian positive definite, thus allowing the use of a very simple double CG. Both systems in this formulation are solved separately, leading to the storage of $N_S(N_S + 1)$ real numbers. The numerical results have displayed a threshold for the discrepancy between the l.h.s. and r.h.s. in identity (3.9), due to the discretization error and beyond which it is, most of the time, unecessary to carry on with the iterations. The value of this threshold constitutes an indicator of the accuracy with which the IE systems are solved. These characteristics remain unchanged when the IE formulation is coupled to the FEM through the DDM. The numerical experiments have shown that the total number of CG2 iterations is of the order of $L \times n_{GC2}(\ell = 1)/2$, on account of the fact that the solutions computed at iteration $(\ell - 1)$ are used as initial solutions for iteration ℓ.

—As a result, for an electrically large object, the memory storage required by this hybrid method corresponds, essentially, to the storage of N_S^2 real numbers and can be further reduced if the fast multipole algorithm is implemented [26, 27]. Also, the numerical experiments have validated the fully iterative procedure that has been employed in this paper for the solution of this DDM algorithm. Obviously, iterative solvers more sophisticated than the very simple CGs implemented here should be experimented with, but this is beyond the scope of this paper.

The main drawback of this technique resides in the fact that the IE systems must be solved L times. L increases when N increases: $L > N$, otherwise the solution in Ω_1 remains unaffected by the spurious reflections due to the TC on S_N [14]. Also, L increases when the innermost interface S_1 is close to the surface of the object, as it has been described in Section V.4, or when weakly attenuated surface waves are present on one of the interfaces S_i, on account of the low efficiency of the TC for waves in grazing incidence [13]. For the latter case, a trivial remedy consists in moving S_i. For instance, if strong creeping waves are propagating on the outermost surface of the materials coating the object, a free-space region can be inserted into the last subdomain between this surface and the surface $S_N = S$ terminating the computational domain. As a general rule, it has been found that L is on the order of 10 when $N \leq 4$ (see also [14]).

Lastly, let us mention that the second-order conformal ABC proposed in [24] constitutes a cheap and memory-efficient, although less accurate, alternative to the IE, that has proved to be interesting for some applications.

APPENDIX A

First, we define the operators $K_\pm$ and $D_\pm$. Then, we show that identity (3.9) is exactly satisfied when the discretization error goes to zero.

$K_\pm$ and $D_\pm$ are defined by

$$K_\pm \Phi(\underline{r}) = \nabla\times\int_S \Phi(\underline{r}')g_r(\underline{r},\underline{r}')\,d\underline{r}' \mp \frac{1}{k}\nabla\times\nabla\times\int_S \Phi(\underline{r}')g_r(\underline{r},\underline{r}')\,d\underline{r}' - \frac{1}{2}\underline{n}(\underline{r})\times\Phi(\underline{r}) \tag{A1a}$$

$$D_\pm \Phi(\underline{r}) = 2k^2\left\{\mp\nabla\times\int_S \Phi(\underline{r}')g_i(\underline{r},\underline{r}')\,d\underline{r}' + \frac{1}{k}\nabla\times\nabla\times\int_S \Phi(\underline{r}')g_i(\underline{r},\underline{r}')\,d\underline{r}'\right\}. \tag{A1b}$$

In the following, ϵ denotes the discretization error, and quantities with the subscript ϵ designate discretized quantities. Let us define by $\Delta_{\epsilon\pm}$ the discrepancy to identity (3.4)

$$X'_{\epsilon\pm} = \mp\frac{i}{2k}X_{\epsilon\pm} + \frac{\Delta_{\epsilon\pm}}{2k}. \tag{A2}$$

The second equation of the discretized system (3.1) reads

$$-k\left(K^H_{\epsilon\pm} \mp i\beta I\right)X_{\epsilon\pm} + 2k^2\beta X'_{\epsilon\pm} + D_{\epsilon\pm}X'_{\epsilon\pm} = 0.$$

Substituting to $X'_{\epsilon\pm}$ the definition (A2) yields

$$-K^H_{\epsilon+}X_{\epsilon+} + \beta\Delta_{\epsilon+} - \frac{i}{2k^2}D_{\epsilon+}X_{\epsilon+} + \frac{1}{2k^2}D_{\epsilon+}\Delta_{\epsilon+} = 0$$
$$-K^H_{\epsilon-}X_{\epsilon-} + \beta\Delta_{\epsilon-} + \frac{i}{2k^2}D_{\epsilon-}X_{\epsilon-} + \frac{1}{2k^2}D_{\epsilon-}\Delta_{\epsilon-} = 0.$$

Adding or substracting the two above equations, we get

$$-\left(K^H_{\epsilon+}X_{\epsilon+} + K^H_{\epsilon-}X_{\epsilon-}\right) - \frac{i}{2k^2}(D_{\epsilon+}X_{\epsilon+} - D_{\epsilon-}X_{\epsilon-}) + \beta(\Delta_{\epsilon+} + \Delta_{\epsilon-}) + \frac{1}{2k^2}(D_{\epsilon+}\Delta_{\epsilon+} + D_{\epsilon-}\Delta_{\epsilon-}) = 0 \tag{A3a}$$

$$i\left(K^H_{\epsilon+}X_{\epsilon+} - K^H_{\epsilon-}X_{\epsilon-}\right) - \frac{1}{2k^2}(D_{\epsilon+}X_{\epsilon+} + D_{\epsilon-}X_{\epsilon-}) - i\beta(\Delta_{\epsilon+} - \Delta_{\epsilon-}) - \frac{i}{2k^2}(D_{\epsilon+}\Delta_{\epsilon+} - D_{\epsilon-}\Delta_{\epsilon-}) = 0. \tag{A3b}$$

On the other hand, if $(\underline{E}^s, \underline{H}^s)$ designates the exact scattered field solution of the problem considered in Section III.2, let us define the field $(\tilde{\underline{E}}^s, \tilde{\underline{H}}^s)$ for $\underline{r} \in R^3\backslash S$ by

$$\tilde{\underline{E}}^s(\underline{r}) = -\nabla\times\int_S(\underline{E}^s\times\underline{n})(\underline{r}')g(\underline{r},\underline{r}')\,d\underline{r}' + \frac{i}{k}\nabla\times\nabla\times\int_S(\underline{H}^s\times\underline{n})(\underline{r}')g(\underline{r},\underline{r}')\,d\underline{r}'$$
$$\tilde{\underline{H}}^s(\underline{r}) = -\nabla\times\int_S(\underline{H}^s\times\underline{n})(\underline{r}')g(\underline{r},\underline{r}')\,d\underline{r}' - \frac{i}{k}\nabla\times\nabla\times\int_S(\underline{E}^s\times\underline{n})(\underline{r}')g(\underline{r},\underline{r}')\,d\underline{r}'$$

with

$$g(\underline{r}, \underline{r}') = g_r(\underline{r}, \underline{r}') - i g_i(\underline{r}, \underline{r}').$$

We know that $\tilde{\underline{E}}^s(\underline{r}) = \underline{E}^s(\underline{r})$, $\tilde{\underline{H}}^s(\underline{r}) = \underline{H}^s(\underline{r})$ for $\underline{r}$ in the exterior of S, and $\tilde{\underline{E}}^s(\underline{r}) = \tilde{\underline{H}}^s(\underline{r}) = 0$ for $\underline{r}$ in the interior of S. As a consequence, if $\underline{r}^- = \lim_{\alpha \to} 0 + (\underline{r} - \alpha \underline{n})$, $\underline{r} \in S$, we have

$$\begin{aligned}\tilde{\underline{E}}^s(\underline{r}^-) = {} & -\nabla \times \int_S (\underline{E}^s \times \underline{n})(\underline{r}')g(\underline{r}, \underline{r}')\, d\underline{r}' \\ & + \frac{i}{k} \nabla \times \nabla \times \int_S (\underline{H}^s \times \underline{n})(\underline{r}')g(\underline{r}, \underline{r}')\, d\underline{r}' + \frac{1}{2}(\underline{n} \times \underline{n} \times \underline{E}^s)(\underline{r}) \qquad \text{(A4a)} \\ \tilde{\underline{H}}^s(\underline{r}^-) = {} & -\nabla \times \int_S (\underline{H}^s \times \underline{n})(\underline{r}')g(\underline{r}, \underline{r}')\, d\underline{r}' \\ & - \frac{i}{k} \nabla \times \nabla \times \int_S (\underline{E}^s \times \underline{n})(\underline{r}')g(\underline{r}, \underline{r}') d\underline{r}' + \frac{1}{2}(\underline{n} \times \underline{n} \times \underline{H}^s)(\underline{r}) \qquad \text{(A4b)}\end{aligned}$$

and

$$\tilde{\underline{E}}^s(\underline{r}^-) = \tilde{\underline{H}}^s(\underline{r}^-) = 0. \qquad \text{(A4c)}$$

For the discretized field $(\underline{E}^s_\epsilon, \underline{H}^s_\epsilon)$ solution of the discretized system (3.5), we have, from the definition in (3.6a)

$$X_{\epsilon\pm} = \left(\tilde{\underline{E}}^s_\epsilon \pm i \underline{H}^s_\epsilon\right) \times \underline{n}.$$

Then, it is easy to show from (A1a, b), (A4a, b) that

$$\begin{aligned} -\left(K^H_{\epsilon+} X_{\epsilon+} + K^H_{\epsilon-} X_{\epsilon-}\right) - \frac{i}{2k^2}(D_{\epsilon+} X_{\epsilon+} - D_{\epsilon-} X_{\epsilon-}) &= 2\tilde{\underline{E}}^s_\epsilon(\underline{r}^-) \\ i\left(K^H_{\epsilon+} X_{\epsilon+} - K^H_{\epsilon-} X_{\epsilon-}\right) - \frac{1}{2k^2}(D_{\epsilon+} X_{\epsilon+} + D_{\epsilon-} X_{\epsilon-}) &= 2\tilde{\underline{H}}^s_\epsilon(\underline{r}^-) \end{aligned}$$

and (A3a, b) can be written as

$$\begin{aligned} \tilde{\underline{E}}_\epsilon(\underline{r}^-) + \frac{\beta}{2}(\Delta_{\epsilon+}(\underline{r}) + \Delta_{\epsilon-}(\underline{r})) + \frac{1}{4k^2}[(D_{\epsilon+}\Delta_{\epsilon+})(\underline{r}) + (D_{\epsilon-}\Delta_{\epsilon-})(\underline{r})] &= 0 \\ \tilde{\underline{H}}_\epsilon(\underline{r}^-) - \frac{i\beta}{2}(\Delta_{\epsilon+}(\underline{r}) - \Delta_{\epsilon-}(\underline{r})) - \frac{i}{4k^2}[(D_{\epsilon+}\Delta_{\epsilon+})(\underline{r}) - (D_{\epsilon-}\Delta_{\epsilon-})(\underline{r})] &= 0. \end{aligned}$$

Combining the two above equations, we get

$$\begin{aligned} \beta \Delta_{\epsilon+}(\underline{r}) + \frac{1}{2k^2}(D_{\epsilon+}\Delta_{\epsilon+})(\underline{r}) &= -(\tilde{\underline{E}}_\epsilon(\underline{r}^-) + i\tilde{\underline{H}}_\epsilon(\underline{r}^-)) \\ \beta \Delta_{\epsilon-}(\underline{r}) + \frac{1}{2k^2}(D_{\epsilon-}\Delta_{\epsilon-})(\underline{r}) &= -(\tilde{\underline{E}}_\epsilon(\underline{r}^-) - i\tilde{\underline{H}}_\epsilon(\underline{r}^-)). \end{aligned}$$

Finally, performing the Hermitian inner product of the first (respectively second) equation by $\Delta_{\epsilon+}$ (respectively $\Delta_{\epsilon-}$) and using the first identity in (3.3b), we arrive at

$$\begin{aligned} \beta\|\Delta_{\epsilon+}\|^2 + \frac{1}{2k^2}\|\delta_{\epsilon+}\Delta_{\epsilon+}\|^2_\infty &= -(\Delta_{\epsilon+},\ \tilde{\underline{E}}_\epsilon(\underline{r}^-) + i\tilde{\underline{H}}_\epsilon(\underline{r}^-)) \\ \beta\|\Delta_{\epsilon-}\|^2 + \frac{1}{2k^2}\|\delta_{\epsilon-}\Delta_{\epsilon-}\|^2_\infty &= -(\Delta_{\epsilon-},\ \tilde{\underline{E}}_\epsilon(\underline{r}^-) - i\tilde{\underline{H}}_\epsilon(\underline{r}^-)). \end{aligned} \qquad \text{(A5)}$$

On account of (A4c), $\lim_{\epsilon\to 0}\tilde{E}^s_\epsilon(\underline{r}^-) = \tilde{H}^s_\epsilon(\underline{r}^-) = 0$ and, since $0 < \beta < 1$, (A5) shows that the values of $\Delta_{\epsilon+}$, $\Delta_{\epsilon-}$ go to zero when the discretization error goes to zero.

ACKNOWLEDGMENTS

We are greatly indebted to Martine Mognot who has realized the finite element meshes needed for the numerical calculations presented in this paper.

REFERENCES

1. X. Yuan, Three-dimensional electromagnetic scattering from inhomogeneous objects by the hybrid moment and finite element method, *IEEE Trans. Microwave Theory Tech.* **MTT-38**, 1053 (1990).
2. W. E. Boyse and A. A. Seidl, A hybrid finite element method for near bodies of revolution, *IEEE Trans. Mag.* **27**, 3833 (1991).
3. B. Stupfel, R. Le Martret, P. Bonnemason, and B. Scheurer, Combined boundary-element and finite-element method for the scattering problem by axisymmetrical penetrable objects, in *Proceedings of the international Symposium on Mathematical and Numerical Aspects of Wave Propagation Phenomena* (SIAM, Philadelphia, 1991). p. 332.
4. P. Soudais, Computation of the electromagnetic scattering from complex 3D objects by a hybrid FEM/BEM method, *J. Electromag. Waves Appl.* **9**, 871 (1995).
5. X. Q. Sheng, J. M. Jin, J. Song, C. C. Lu, and W. C. Chew, On the formulation of hybrid finite-element and boundary-integrals method for 3-D scattering, *IEEE Trans. Antennas Prop.* **AP-46**, 303 (1998).
6. R. Lee and V. Chupongstimun, A partitioning technique for the finite element solution of electromagnetic scattering from electrically large dielectric cylinders, *IEEE Trans. Antennas Prop.* **AP-42**, 737 (1994).
7. C. T. Spring and A. C. Cangellaris, Parallel implementation of domain decomposition methods for the electromagnetic analysis of guided wave systems, *J. Electromag. Waves Appl.* **9**, 175 (1995).
8. A. Barka, P. Soudais, and D. Volpert, Scattering from 3-D cavities with a plug and play numerical scheme combining IE, PDE and modal techniques, *IEEE Trans. Antennas Prop.* **AP-48**, 704 (2000).
9. C. T. Wolfe, U. Navsariwala, and S. D. Gedney, A parallel finite-element tearing and interconnecting algorithm for solution of the vector wave equation with PML absorbing medium, *IEEE Trans. Antennas Prop.* **AP-48**, 278 (2000).
10. B. Després, Ph.D. dissertation (Université Paris IX Dauphine, France, (1991).
11. B. Després, P. Joly, and J. E. Roberts, A domain decomposition method for the harmonic Maxwell equations, in *Iterative methods in Linear Algebra*, edited by R. Beauwens and P. de Groen, (Elsevier, Amsterdam/New York, 1992), p. 475.
12. P. Collino, S. Ghanemi, and P. Joly, Domain decomposition method for harmonic wave propagation: A general presentation, *Comput. Meth. Appl. Mech. Eng.* **184**, 171 (2000).
13. B. Stupfel, A fast domain decomposition method for the solution of electromagnetic scattering by large objects, *IEEE Trans. Antennas Prop.* **AP-44**, 1375 (1996).
14. B. Stupfel and M. Mognot, A domain decomposition method for the vector wave equation, *IEEE Trans. Antennas Prop.* **AP-48**, 653 (2000).
15. B. Stupfel and B. Despres, A domain decomposition method for the solution of large electromagnetic scattering problems, *J. Electromag. Waves Appl.* **13**, 1553 (1999).
16. B. Stupfel and M. Mognot, Implementation and derivation of conformal absorbing boundary conditions for the vector wave equation, *J. Electromag. Waves Appl.* **12**, 1653 (1998).
17. B. Després, Fonctionnelle quadratique et équations intégrales pour les équations de Maxwell harmoniques en domaine extérieur, *C. R. Acad. Sci. Paris* **323**, Série I, 1145 (1996).
18. F. Collino and B. Després, *Integral Equations via Saddle Point Problems for Time-Harmonic Maxwell's Equations*, Technical Report R00036 (Laboratoire d'Analyse Numérique, Université Pierre et Marie Curie, 75252 Paris cedex 05, France, 2000).

19. S. M. Rao, D. R. Wilton, and A. W. Glisson, Electromagnetic scattering by surfaces of arbitrary shape, *IEEE Trans. Antennas Prop.* **AP-30**, 409 (1982).

20. P. Bonnemason, Résolution par formulations intégrales du problème de la diffraction d'une onde électromagnétique par des objets 3D conducteurs recouverts ou non de matériaux, *Proceedings of the Journées Européennes sur les méthodes numériques en électromagnétisme, Nov. 1993* (Toulouse, France), p. 185.

21. V. H. Weston, Theory of absorbers in scattering, *IEEE Trans. Antennas Prop.* **AP-11**, 578 (1963).

22. P. Bonnemason and B. Stupfel, Modeling high frequency scattering by axisymmetric perfectly or imperfectly conducting scatterers, *Electromagnetics* **13**, 111 (1993).

23. M. Mandallena, Modélisation d'antennes plaquées par méthodes intégrales, in *Proceedings of Atelier de travail CNES: Méthodes numériques pour la modélisation d'antennes, October 1996* (Toulouse, France).

24. B. Stupfel, Absorbing boundary conditions on arbitrary boundaries for the scalar and vector wave equations, *IEEE Trans. Antennas Prop.* **AP-42**, 773 (1994).

25. J. Liu and J. M. Jin, A special higher-order finite-element method for scattering by deep cavities, *IEEE Trans. Antennas Prop.* **AP-48**, 694 (2000).

26. J. M. Song, C. C. Lu, W. C. Chew, and S. W. Lee, Fast Illinois solver code (FISC), *IEEE Trans. Antennas Prop. Mag.* **40**, 27 ((1998).

27. K. Mer, The fast multipole method applied to a mixed integral system for time-harmonic Maxwell's equations, in *Proceedings of the Second International Conference on Boundary Integral Methods: Theory and Applications, Bath, Great-Britain, September 2000.*